Asian Pacific Journal of Tropical Biomedicine

Journal homepage: www.apjtb.org

doi: 10.4103/2221-1691.239425

Biomolecular changes and DNA targeting effect of sesamol in human lung adenocarcinoma (SK-LU-1) cells by FTIR microscopy

Boondaree Siriwarin[1], Natthida Weerapreeyakul[2]✉, Waraporn Tanthanuch[3], Kanjana Thumanu[3]

[1]*Graduate School (Research and Development in Pharmaceuticals Program), Faculty of Pharmaceutical Sciences, Khon Kaen University, Khon Kaen, 40002, Thailand*

[2]*Faculty of Pharmaceutical Sciences, Khon Kaen University, Khon Kaen, 40002, Thailand*

[3]*Synchrotron Light Research Institute (Public Organization), Nakhon Ratchasima, 30000, Thailand*

ARTICLE INFO

Article history:
Received 5 May 2018
Revision 8 June 2018
Accepted 20 July 2018
Available online 23 August 2018

Keywords:
FTIR microscopy
Sesamol
Cisplatin
Lung adenocarcinoma
Biomolecular change

ABSTRACT

Objective: To investigate biomolecular alteration of sesamol on human lung adenocarcinoma (SK-LU-1) cells compared with cisplatin using Fourier transform infrared microscopy (FTIR). **Methods:** Cytotoxicity of sesamol was investigated against SK-LU-1 cells by using neutral red. DNA fragmentation and the cell cycle analysis were determined by agarose gel electrophoresis and flow cytometry, respectively. The FTIR microscopy technique was applied to explore the changes in cellular biochemical compositions in cells treated with sesamol that the biochemical and biological assays cannot cover. The alkylating property was determined by 4-(4-nitrobenzyl)pyridine assay. **Results:** Sesamol and cisplatin exerted an antiproliferative effect at 48 h with respective IC_{50} values of 2.7 and 0.07 mM. Both induced apoptosis by causing DNA damage and accumulation of cell populations at sub-G_1. FTIR microscopy and Principle Component Analysis clearly discriminated the sesamol- and cisplatin-treated cells from the untreated cells or control. A significant increase of total lipid content was found in cisplatin-treated cells. Conformational changes in the proteins secondary structure from the α-helix to the β-sheet were found in both sesamol- and cisplatin-treated cells, as well as significant reductions in relative DNA content of both compared to the control were observed, suggesting DNA damage. A shift in the peak position of DNA region provides insight on the DNA interactions. **Conclusions:** The non-alkylating effect of sesamol based on the nitrobenzyl pyridine assay delineates the non-covalent binding mode of sesamol on DNA. Hydrogen bonding is the binding mode of sesamol on DNA, while for cisplatin it was covalent and hydrogen bonding.

1. Introduction

DNA is the essential part that carries genetic information and DNA damage will lead to mutation, which can be carcinogenic. Many anticancer agents directly target with DNA or prevent DNA relaxation in the DNA replication process[1]. The discovery or characterization of DNA-targeting compounds is, therefore, of

✉Corresponding author: Natthida Weerapreeyakul, Faculty of Pharmaceutical Sciences, 123 Mittrapap Road, Amphoe Muang, Khon Kaen University, Khon Kaen, 40002, Thailand.
Tel: +66 43 202 378
Fax: +66 43 202 379
E-mail: natthida@kku.ac.th

Foundation project: This work was supported by the Higher Education Research Promotion and National Research University Project of Thailand, Office of the Higher Education Commission, through the Food and Functional Food Research Cluster and Research and Development of Herbal Nutraceutics Subcluster of Khon Kaen University (FC 3.1.13 PhD and NRU 541057).

How to cite this article: Siriwarin B, Weerapreeyakul N, Tanthanuch W, Thumanu K. Biomolecular changes and DNA targeting effect of sesamol in human lung adenocarcinoma (SK-LU-1) cells by FTIR microscopy. Asian Pac J Trop Biomed 2018; 8(8): 377-386.

interest for overcoming cancer. The bonding between anticancer agents and DNA interaction are covalent binding or cross-linking, non-covalent groove binding and intercalation[2]. These interactions result in alteration to thermodynamic stability and DNA functions[3]. The predominant interactions of small molecules to DNA are intercalation and minor groove binding. Intercalating molecules typically have a planar and aromatic structure, which fits between base pairs, while pyrrole-, furan- or benzene-containing structures bind to the DNA minor groove[4].

Sesamol is a small phenolic derivative of lignans, possessing (a) anticancer activity against various cancer cell lines[4–6], (b) a radio-protective effect against DNA damage, (c) ROS-scavenging activity[7,8], and (d) a radiosensitizer for human cervical cancer cells[9]. In addition, sesamol induced HepG2 cells to undergo apoptosis, resulting in DNA fragmentation[4]. We recently reported the mechanism of anticancer action of sesamol which was by inducing apoptosis through both intrinsic and extrinsic pathways in SK-LU-1 cells[10]. The effect of sesamol *in silico*-molecular docking suggests that sesamol may be deposited in the minor groove of DNA[4]. The effect of sesamol on cellular composition especially on the DNA structure of lung cancer cell line has yet to be elucidated. The present work is extended from the previous study by using techniques to assess the DNA damage (*i.e.* fragmentation). The application of Fourier transform infrared (FTIR) microscopy is proposed in this manuscript to solve the research question that the biochemical assay and biological assay cannot cover.

FTIR microscopy has been used to probe for the DNA structure of various compounds[11]. The infrared will interact with the cell samples. The vibrational modes of the functional groups of the cellular biological molecules are subsequently measured[12]. One of advantage of this technique is that it is a nondestructive technique for analysis of all macromolecules inside a cell population. FTIR microscopy has also been used to analyze various biomolecular events in the integrated sciences with fast speed, relatively inexpensive cost and automated-data acquisition time[13–15]. Due to its sensitivity, FTIR microscopy can monitor the mode of apoptotic cell death in human leukemic cells[15], and the structural and intracellular changes in lung cancer cells compared to noncancerous human bronchial epithelial cells[14]. FTIR microscopy has, moreover, been used to detect the antimelanogenic effect of sesamol and its biomolecular changes in human melanoma cells[16]. FTIR microscopy was thus adapted to characterize the biomolecular changes in, and interactions with, the DNA in SK-LU-1 cells caused by sesamol compared with standard intercalating cisplatin, and to ascertain DNA interaction with the two compounds. In the current study, FTIR microscopy was adopted to investigate the effect of sesamol on biomolecular changes within the cells and to characterize the interaction with the DNA. The information derived from this experiment is needed in order to understand the putative DNA-targeting anticancer function via the cellular response to sesamol.

2. Materials and methods

2.1. Cell culture and chemicals

Sesamol (98% purity) was bought from Spectrum (New Brunswick, NJ, USA). Cisplatin was from Boryung Pharmaceutical (Ansan, Korea). Cisplatin has been recommended for the treatment of non-small cell lung cancer according to the NCCN Guidelines and used as a positive control. Melphalan was purchased from Sigma-Aldrich Chemie GmbH (Eschenstraße, Taufkirchen, Germany). The reagents used in the cell-based assay were molecular biological grade. Dulbecco's Modified Eagle's Medium (DMEM), fetal bovine serum, penicillin, and streptomycin were from GIBCO® (Invitrogen, Grand Island, NY, USA). Neutral red (NR) was from Sigma-Aldrich (Saint Louis, MO, USA). The FlexiGene DNA kit was purchased from QIAGEN (Hilden, Germany). Ethidium bromide was purchased from Applichem GmbH (Darmstadt, Germany). Agarose (biotechnology grade) was from Bio-Rad (Solon, OH, USA), and 100 bp+1.5 Kb DNA ladder with stain was from SibEnzyme (Novosibirsk, Russia). Sodium chloride (NaCl) was obtained from Ajax Finechem (Auckland, New Zealand).

2.2. Cytotoxic assay

Human lung adenocarcinoma cisplatin-sensitive (SK-LU-1) cell line was obtained from Cell Lines Service (CLS#300335, Eppelheim, Germany). The DMEM media was supplemented with 10% fetal bovine serum, 100 U/mL penicillin and 100 μg/mL streptomycin. Cells were incubated in a 5% CO_2 incubator at 37 ℃.

Briefly, cells were seeded at 4×10^5 cells/mL in 96 well microplates. The cells were then treated with various concentrations of sesamol or cisplatin for 48 h. At the end of the treatment, the cells were incubated with NR solution for 2 h (final concentration of 50 μg/mL). Afterward, the cells were rinsed with phosphate buffered saline (PBS) (150 μL) and the supernatant was discarded. HCl/isopropanol (0.33% w/v) was then added to each well to dissolve the cells. Absorbance was determined at dual wavelength 537 nm and a reference wavelength of 650 nm, using a microplate photometer (Tecan, Lyon, France).

Percentage of cytotoxicity was calculated vis-à-vis the control (untreated cells). Similar NR assay was performed for the other cell lines including human melanoma cells (SK-MEL-2), human cervical adenocarcinoma cells (HeLa), human cervical squamous cell carcinoma cells (SiHa), human lung adenocarcinoma cell (SK-LU-1), and noncancerous African green monkey kidney cells (Vero).

2.3. DNA ladder assay

DNA fragmentation assay presented as DNA ladder was used to determine late-stage apoptosis induction. Briefly, the cells were treated with sesamol or cisplatin (at concentration of $2 \times IC_{50}$) with exposure time of 48 h. To better identify the anticancer effect of the test compounds on cells and biochemical changes, a two-fold concentration ($2 \times IC_{50}$ value) was employed. Cells in the control group were treated with culture medium. The cells were trypsinized and washed with PBS. The DNA was extracted from the treated cells using a DNA Kit (QIAGEN, Hilden, Germany) and electrophoresed on 1.8% agarose gel with 0.1 mg/mL ethidium bromide. DNA fragmentation of apoptotic cells was detected using the Gel Documentation (Syngene, Frederick, MD, USA).

2.4. Analysis of cell cycle

Flow cytometry was used to analyze the effect of sesamol on cell cycle phases distribution. Cells were seeded and treated with 1 × IC_{50} (2.7 mM) and 2 × IC_{50} (5.4 mM) of sesamol for 24 and 48 h. Afterward the cells were collected and rinsed with cold PBS. The cell pellet was fixed in 100% ethanol for 30 min at -20 ℃. After washing with PBS, the cells pellet was stained with propidium iodide (50 μg/mL) consisting of RNase A (100 μg/mL) for 30 min in the dark. The DNA content was measured using a flow cytometer (BD FACSCanto Ⅱ, San Jose, CA, USA) and the percentages of G_0/G_1, S, and G_2/M cells were calculated.

2.5. FTIR microscopy for biomolecular changes

SK-LU-1 untreated cells (control), and cells treated with sesamol 5.4 mM and cisplatin 0.14 mM (positive control) for 48 h were considered for the analysis. Experiments were done in triplicate, and each replica was independently measured by FTIR microscopy. Cells were collected and washed by adding 0.9% NaCl dropwise on low-e slides (MirrIR, Kevley Technologies, Chesterland, OH, USA) and dried under negative pressure for 10 min in an airtight container. These dried cells were rinsed off with distilled water to remove the excess NaCl precipitate and dry under vacuum. This step was repeated until a thin monolayer of cells was obtained and observed under an inverted microscope. This will provide the FTIR absorbance to be lesser than 1. The slide of the cell monolayer was kept under the desiccator for FTIR microscopy.

FTIR microscopy was used to assess biochemical changes in the SK-LU-1 cells. Measurements were performed by an off-line FTIR microscopy at the IR-end station of Synchrotron Light Research Institute, Thailand. A Bruker Vertex 70 spectrometer was used for FTIR data acquisition. The Bruker Hyperion 2000 microscope (Bruker Optics Inc., Ettlingen, Germany) had a 36 × IR objective lens with a nitrogen cooled MCT (HgCdTe) detector. The obtained FTIR spectra were in the reflection mode from 64 scans. An aperture size (68 μm × 68 μm) at a resolution of 4 cm^{-1} was engaged to cover the detected range of 4 000–600 cm^{-1}. Spectral acquisition and instrument control were conducted using the OPUS 6.5 software (Bruker Optics Ltd, Ettlingen, Germany).

Principal Component Analysis (PCA) was used to identify any significant differentiation between the data sets. PCA was performed using the Unscrambler software (version 9.7, CAMO Software AS, Oslo, Norway) with a spectral range of 3 000–2 800 cm^{-1} and 1 800–900 cm^{-1}. Spectral data were taken for the second derivative using the Savitzky–Golay algorithm with 9 points of smoothing; thereby minimizing the effects of variable baselines. The spectra were normalized to account for differences in sample thickness. Extended multiplicative signal correction was performed to correct the scattering artifacts. The principal components (PCs) were analyzed. Score plots (2D) and loading plots represented the clustering and deviation in the data.

The OPUS 6.5 software was used to integrate the peak areas. The peak areas of lipids (3 000–2 800 cm^{-1}), amide Ⅰ (1 700–1 600 cm^{-1}), amide Ⅱ (1 600–1 500 cm^{-1}), carbohydrate and nucleic acids (1 300–900 cm^{-1}) were calculated as percentage of relative integrated peak area and represented on histograms. Curve fitting was analyzed from the amide Ⅰ region (1 710–1 590 cm^{-1}) to differentiate the secondary structure of proteins. A multi-peak fitting program with Gaussian and Lorentzian functions from the OPUS 6.5 software was performed to quantify the multicomponent peak areas in the protein amide Ⅰ bands with the Levenberg-Marquardt Algorithm. Voigt curves (*i.e.*, a mix of Gaussian and Lorentz) was used for fitting. The percentage of Gaussian and Lorentian was fixed during the fitting at 50%. The parameters, the peak positions or wavenumbers, were obtained from second derivative analysis to find the real peak position in amide Ⅰ region for curve fitting. The fixed parameter was the peak position, while the varied parameters were the peak intensity and width. The goodness of fit was determined by assessing the residual RMS error.

The spectra used for the curve fitting were obtained from the average spectra of each treatment groups. The curve fitting provided the average ± SD of the peak position and its integral area with the following criteria. If there were a shift of the peak position more than ±4 cm^{-1}, it was considered a significant shift when compared to the control. The statistical analysis of the difference between integral areas was performed using a one-way ANOVA in SPSS (P<0.05).

2.6. Alkylation assay

To evaluate the alkylating properties of compounds, 4-(4-nitrobenzyl)pyridine (NBP) was used to represent nucleophile 7-alkylguanine. NBP can be alkylated to produce a pyridinium salt, which produces a blue color in alkaline media. NBP was thus used to determine the alkylating interaction between potential antineoplastic compounds and the DNA target. The NBP assay was performed as per Machana *et al*., 2011[17]. Cisplatin, however, had limited solubility so only 3 mM could be used. Melphalan (30 mM)—an alkylating chemotherapeutic agent—was, therefore, used as the positive control, while 5-fluorouracil (5-FU) was the negative control. Briefly, 52 mM sesamol, 77 mM 5-fluorouracil (5-FU), and 3 mM cisplatin or 30 mM melphalan (positive control) were mixed with NBP and citrate buffer solution (pH 4.0), then incubated at 70 ℃ for 5-30 min. The mixture solutions were pipetted into test plates in an ice bath and mixed in a 1:1 ratio of absolute ethanol and 0.1 N sodium hydroxide. The alkylated product appeared blue and the intensity of the developed blue color was measured at 600 nm with a microplate photometer (Tecan, Lyon, France).

2.7. Statistical analysis

The average of treatment groups (±SD) was calculated compared to the control. One-way ANOVAs (SPSS, USA) were used to compare the sesamol- and cisplatin-treatment groups with the control. Statistical significance within the 95% level of confidence interval was set at P<0.05.

3. Results

3.1. Cytotoxic effect

The cytotoxicity of sesamol was evaluated by using the NR

assay in various cancer cell lines including SK-MEL-2, HeLa, SiHa, SK-LU-1 and Vero. After treatment, sesamol exerted the highest cytotoxicity in SK-LU-1. The cytotoxicity depended on a concentration with an IC_{50} of 2.7 mM in SK-LU-1 followed by SK-MEL-2 (3.0 mM), HeLa (>5 mM), and SiHa (>5 mM) (Figure 1A). Thus, SK-LU-1 cell line was chosen for further experiments due to the highest sensitivity to sesamol. Selective cytotoxicity of sesamol and cisplatin to SK-LU-1 cells was evaluated compared with Vero cells (Figure 1B and 1C). Sesamol exhibited a cytotoxic effect with an IC_{50} of 7.6 mM in Vero cells whereas cisplatin exhibited an IC_{50} of 0.07 mM in SK-LU-1 and Vero cells. Sesamol, thus, possessed higher selectivity in SK-LU-1 cells than cisplatin.

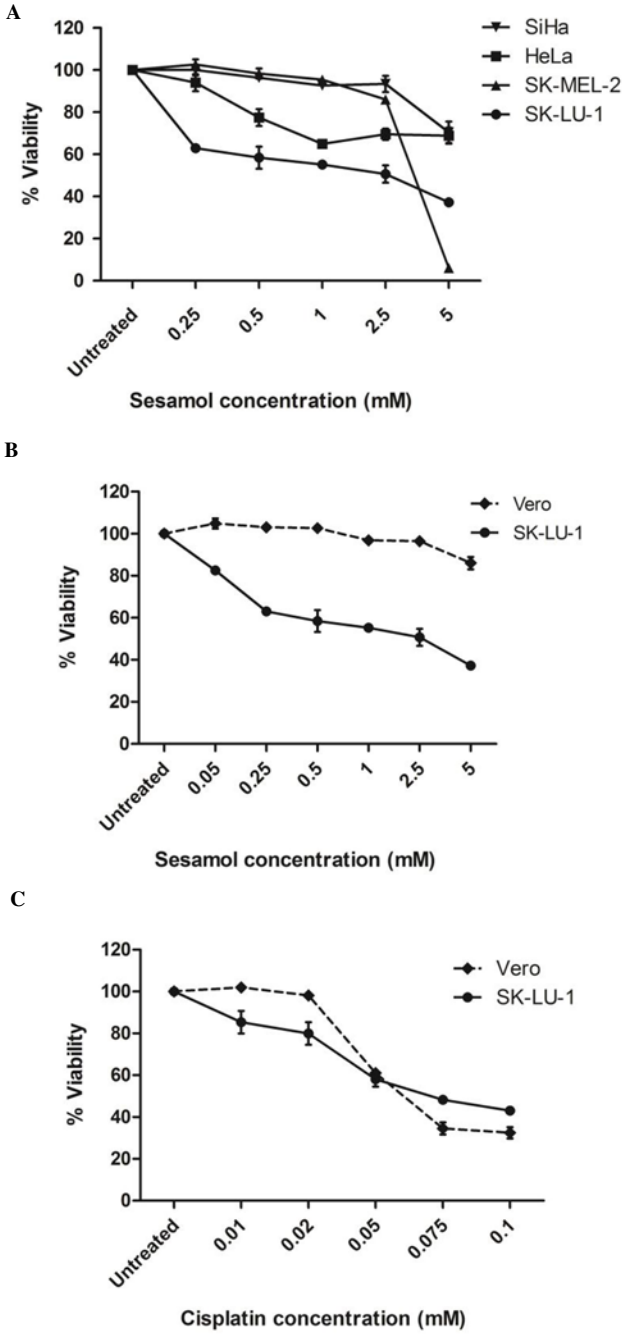

Figure 1. Anticancer activity of sesamol.
(A) Cytotoxicity of sesamol on the four different cancer cell lines, SK-MEL-2, HeLa, SiHa, and SK-LU-1 at 48 h by NR assay. (B) Selective cytotoxicity of sesamol and (C) cisplatin on SK-LU-1 cells compared with Vero cells at 48 h.

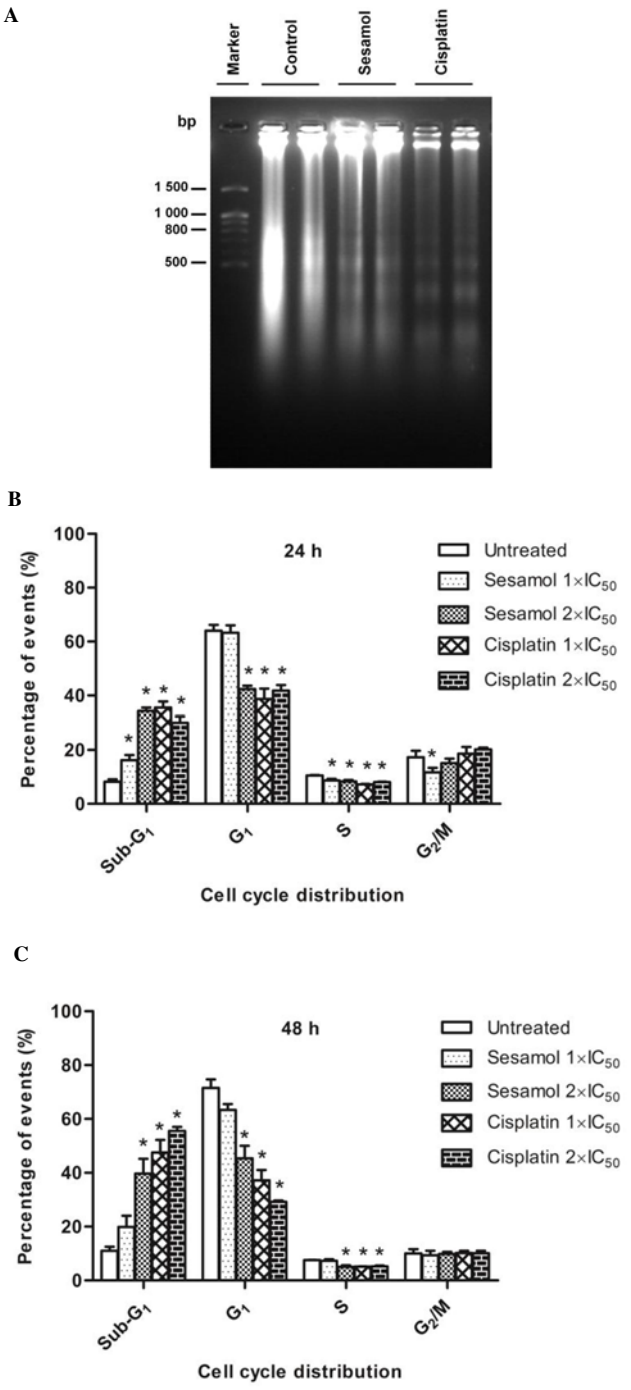

Figure 2. DNA fragmentation and cell cycle distribution.
(A) DNA fragmentation in SK-LU-1 cells treated with 2 × IC_{50} sesamol (5.4 mM) and 2 × IC_{50} cisplatin (0.14 mM) at 48 h. (B) Cell cycle distribution in SK-LU-1 cells after treatment with sesamol and cisplatin at 24, and (C) 48 h. $^{*}P<0.05$ compared with untreated cells at 24 and 48 h.

Figure 2A illustrates a ladder pattern of DNA fragmentation in the SK-LU-1 cells treated with sesamol and cisplatin but not in the untreated cells. Results suggested that sesamol and cisplatin caused DNA damage by induction of endonuclease enzyme and eventually induced SK-LU-1 cells death via apoptosis. Here we report the DNA targeting effect of sesamol compared to cisplatin, based on apoptosis inducing mechanism in SK-LU-1 cells.

Figures 2B and 2C show that the SK-LU-1 cells treated with

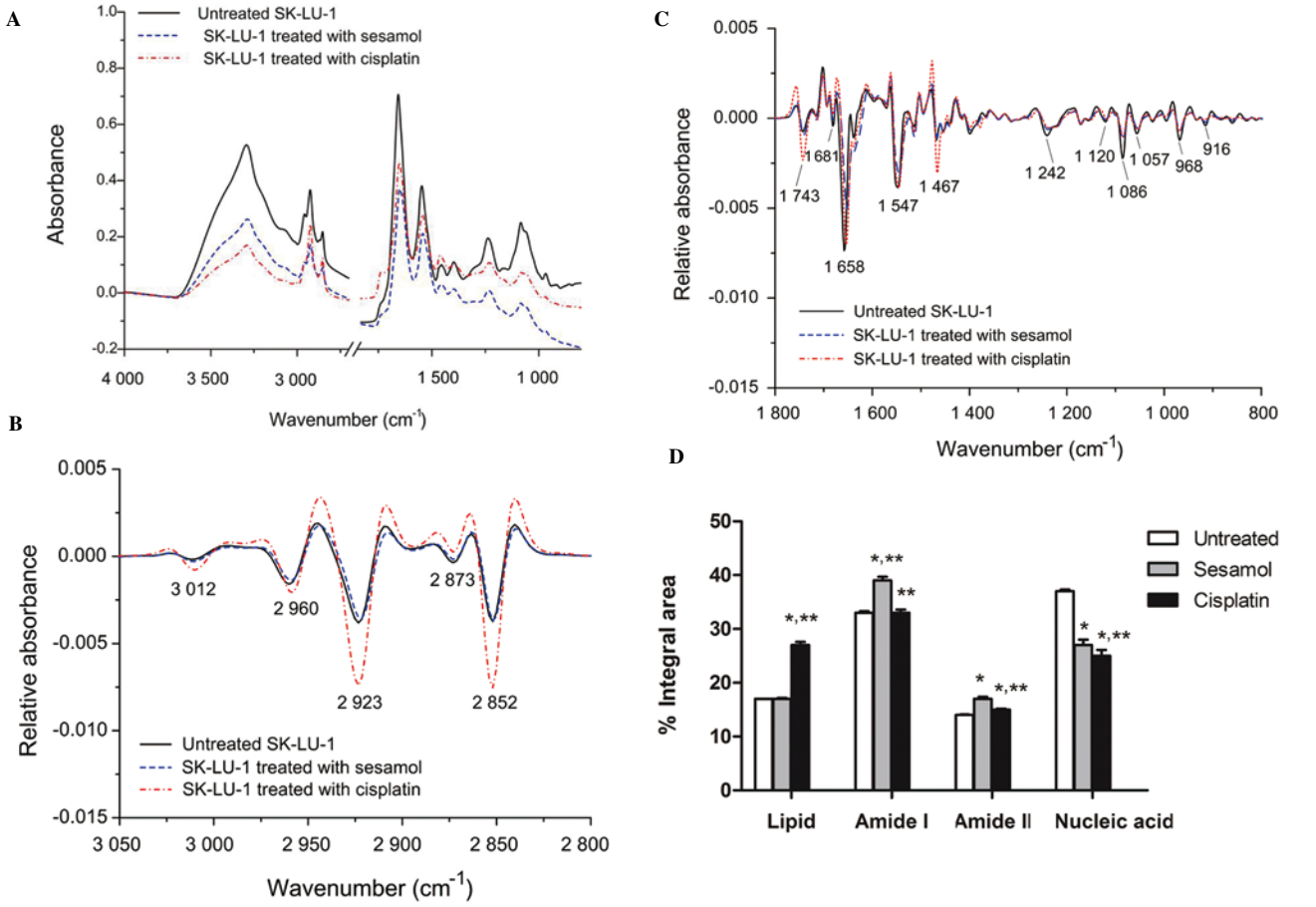

Figure 3. Analysis of untreated– and treated–SK-LU-1 cells using FTIR microscopy.

(A) Average original FTIR spectra (n=217) of SK-LU-1 treated with 2 × IC_{50} sesamol (5.4 mM) (n=88) compared to 2 × IC_{50} cisplatin (0.14 mM) (n=55) and untreated cells (n=74) at 48 h. (B) Average second derivative spectra from experiments at the lipid region (3 000–2 800 cm^{-1}), and (C) protein (1 700–1 500 cm^{-1}) and carbohydrate and nucleic acid regions (1 300–900 cm^{-1}). (D) Histogram presents mean integral area for lipid (3 000–2 800 cm^{-1}), amide Ⅰ (1 700–1 600 cm^{-1}), amide Ⅱ (1 600–1 500 cm^{-1}), and nucleic acid (1 300–900 cm^{-1}) of original spectra. $^{*}P$<0.05 *vs*. untreated cells, $^{**}P$<0.05 sesamol *vs*. cisplatin (one–way ANOVA).

sesamol and cisplatin result in accumulation of hypodiploid cells in the sub-G_1 phase, which indicates an occurrence of DNA fragmentation due to apoptosis induction. Sesamol exhibited an increase in the sub-G_1 population when increasing concentration at 24 h. However, cisplatin exerted effects in a time-dependent manner (Figure 2B and 2C). At 24 h, the percent of cells population accumulated in the sub-G_1 phase was dominantly increased after being treated with 2.7 mM and 5.4 mM of sesamol (16.2%, and 34.3%, respectively) (P<0.05). At 48 h, the percentage of sub-G_1 population in cells treated with 2.7 mM and 5.4 mM of sesamol increased to 19.9% and 39.7%, respectively (P<0.05). At 24 h, the percentages of cells accumulated in the sub-G_1 phase after being treated with 0.07 mM (35.5%) and 0.14 mM (30.0%) cisplatin were significantly higher than the untreated cells (8.2%) (P<0.05). At 48 h, the percentage of sub-G_1 population among cells treated with 0.07 mM and 0.14 mM of cisplatin significantly increased to 47.5%, and 55.5%, respectively (P<0.05). These results show that both sesamol and cisplatin affected cellular DNA (reduced DNA content) causing apoptotic cell death in SK-LU-1 cells together with sub-G_1 phase arrest (predominantly increased sub-G_1 DNA content).

3.2. FTIR microscopy of SK-LU-1 cells

In the current study, the original absorbance FTIR spectra of the untreated and the treated SK-LU-1 cells were obtained between 4 000–600 cm^{-1} (Figure 3A). The biomolecules can be observed in three FTIR-regions comprising the regions of lipid (3 000–2 800 cm^{-1}), protein (1 700–1 500 cm^{-1}), and carbohydrate and nucleic acids (1 300–900 cm^{-1}) (Figure 3A). The average FTIR absorbance spectra of untreated, sesamol-treated, and cisplatin-treated SK-LU-1 cells after normalization to the amide Ⅰ peak are shown in Figure 3A. The average FTIR absorbance spectra were converted to the second derivative in order to differentiate the respective peak band position by visual inspection (Figure 3B and 3C).

The lipid region comprises 4 prominent bands: 3 012 cm^{-1}, 2 960 cm^{-1}, 2 923 cm^{-1} and 2 852 cm^{-1} (Figure 3B). The peak at 3 012 cm^{-1} (the vinyl stretching band) was observed and slightly shifted to 3 010 cm^{-1} in the cells treated with sesamol and cisplatin (Figure 3B). The peak intensity was relatively higher in the cells treated with cisplatin than sesamol and untreated SK-LU-1 cells. The strong bands at 2 923 cm^{-1} and 2 852 cm^{-1} represent the $\nu_{as}CH_2$– of the acyl chains in lipids and the ν_sCH_2– of the acyl chains, respectively. These two bands in cisplatin-treated SK-LU-1 cells had a stronger intensity than the untreated and sesamol-treated cells. The band at 2 960 cm^{-1} represents the asymmetric stretching vibration of CH_3– ($\nu_{as}CH_3$–) of lipids, proteins, and nucleic acids. The cisplatin-treated SK-LU-1 cells illustrated a stronger intensity at 2 960 cm^{-1} than the untreated and sesamol-treated cells. The band at 1 743 cm^{-1} assigned to C=O

Table 1

Positions and the integral area of protein assignments of untreated SK-LU-1 cells and after being treated with sesamol and cisplatin.

Assignment	Untreated		Sesamol		Cisplatin	
	Position (cm^{-1})	Integral area (%)	Position (cm^{-1})	Integral area (%)	Position (cm^{-1})	Integral area (%)
β -sheet	1 625.0±0.4	13.4±0.3	1 619.0±0.2[b]	17.0±0.7[a]	1 623.0±0.8	16.4±0.5[a]
β -sheet	1 641.0±0.2	23.1±0.4	1 634.0±0.2[b]	20.3±0.6[a]	1 637.0±0.6	21.2±0.6[a]
α -helix	1 657.0±0.1	32.1±0.9	1 648.0±0.3[b]	27.9±0.8[a]	1 652.0±0.4[b]	31.8±2.6
β -sheet/Turns	1 671.0±0.2	20.2±1.1	1 662.0±0.3[b]	21.9±1.4	1 665.0±0.6[b]	19.3±0.8
Turns	1 686.0±0.2	11.2±0.3	1 680.0±0.4[b]	12.9±0.6	1 681.0±0.7[b]	11.2±1.6

[a]Integral area statistically significant difference compared with untreated SK-LU-1 cells (P<0.05, one-way ANOVA).

[b]Peak position significant difference compared with untreated SK-LU-1 cells.

stretching mode of lipid exhibited the highest absorption in the cisplatin-treated cells (Figure 3C).

The strong band in the protein regions at 1 658 cm^{-1} (assigned to the α -helix structure), and 1 547 cm^{-1} (assigned to amide Ⅱ from δ N–H and νC–N) showed stronger absorption in untreated cells and cisplatin-treated cells than sesamol-treated cells (Figure 3C). The band at 1 467 cm^{-1} which showed the highest absorption in cisplatin-treated cells represents CH_2 the bending vibration of lipids and proteins.

The carbohydrate and nucleic acid regions comprise many characteristic bands at 1 242 cm^{-1}, 1 120 cm^{-1}, 1 086 cm^{-1}, 1 057 cm^{-1}, 968 cm^{-1}, and 916 cm^{-1} showed stronger intensity in the untreated SK-LU-1 cells than the sesamol- and cisplatin-treated SK-LU-1 cells (Figure 3C). The band at 1 242 cm^{-1}, which was assigned to the PO_2^--asymmetric stretching mode was found in the untreated cells and this band was shifted to 1 240 cm^{-1} for sesamol-treated and cisplatin-treated cells. The remarkable bands in these regions were 1 086 cm^{-1} and 968 cm^{-1}, and peak at 1 086 cm^{-1} was assigned to the symmetric stretching of the phosphate groups of phosphodiester bond in the DNA and RNA, while 968 cm^{-1} was assigned to the C–C/C–O stretching of deoxyribose-ribose vibration. The lower intensity of these bands in the sesamol- and cisplatin-treated SK-LU-1 cells demonstrates a decreased nucleic acid content which is indicative of DNA fragmentation caused by apoptotic cell death.

The histogram (Figure 3D) represents the mean integrated areas of primary spectra of cells treated with sesamol and cisplatin. The biomolecular contents in the cisplatin-treated cells clearly differed from the untreated cells by virtue of an increased lipid and decreased nucleic acid content (P<0.05). Interestingly, sesamol-treated cells showed a decreased carbohydrate and nucleic acid content and increased amide Ⅰ content than the control (P<0.05), but no increase in lipid. In the present study, cisplatin exhibited higher %apoptotic cells than sesamol; thus, the prominent change in the biochemical component of both lipid and nucleic acid levels was observed in cells treated with cisplatin.

The amide Ⅰ content significantly increased in the sesamol-treated cells compared to the control and cisplatin-treated cells. Nucleic acid content was significantly decreased in sesamol- and cisplatin-treated cells compared with the control (P<0.05). A decrease in the overall DNA response in the cells detected by FTIR spectroscopy, agrees with the DNA ladder observed after cells were treated by sesamol and cisplatin (Figure 2A).

In addition to the determination of biomolecular content, more details about the secondary structure of amide Ⅰ was evaluated using curve fitting. The position and integral area of the average original spectra of the amide Ⅰ region (1 710–1 590 cm^{-1}) in the untreated *vs*. treated cells were analyzed. The amide Ⅰ band can be divided into 5 components (Figure 4): the first and second components represented to the β -pleated sheet (1 641–1 619 cm^{-1}); the third component to the α -helix structure (1 657–1 648 cm^{-1}); the fourth to the β -sheet and turns (1 671–1 662 cm^{-1}); and, the fifth to turns (1 686–1 680 cm^{-1}).

The means of the position and integral areas of each treatment group are shown in Table 1. Significant increase of integral area of the β -pleated sheet structure was observed in the sesamol- (17.0%) and cisplatin- (16.4%) treated cells compared to the control (13.4%). The position of the β -sheet structure in the sesamol-treated cells was clearly shifted from the untreated cells (1 625 cm^{-1}) to 1 619 cm^{-1} (Figure 4).

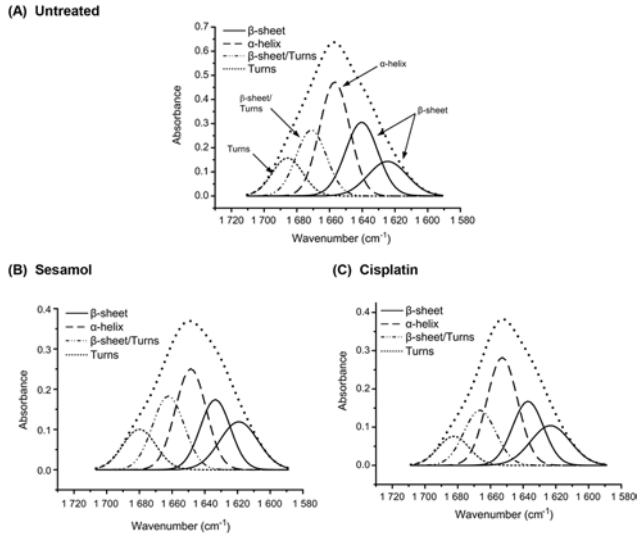

Figure 4. Absorbance of the amide Ⅰ band contour with best-fit 50% Lorentzian/Gaussian individual component bands for (A) untreated SK-LU-1 cells, (B) SK-LU-1 cells treated with sesamol, and (C) SK-LU-1 cells treated with cisplatin.

The significant decrease of an integral area of the α -helix structure was observed in the sesamol-treated cells (27.9%) but non-significant decrease was found in the cisplatin-treated cells (31.8%) vis-à-vis the untreated cells (32.1%). The α -helix structure was, however, dominantly shifted from the control cells (1 657 cm^{-1}) to the sesamol- (1 648 cm^{-1}) and cisplatin-treated cells (1 652 cm^{-1}).

After being treated with sesamol and cisplatin, the integral area of β -sheet/turns was slightly changed and the peak positions of this structure shifted to lower frequency than the untreated cells. The β -sheet/turns structures were significantly shifted from the control (1 671 cm^{-1}) to the sesamol- (1 662 cm^{-1}) and cisplatin-treated cells

(1 665 cm^{-1}). The turn structures were significantly shifted from the control (1 686 cm^{-1}) to the sesamol- (1 680 cm^{-1}) and cisplatin-treated cells (1 681 cm^{-1}).

The increase in the relative integral area of the β-sheet and the decrease in the relative integral area of the α-helix induced by sesamol and cisplatin may be due to the conformational change from the α-helix structure protein to the β-sheet in apoptotic cells. PCA was performed to define the difference between the treated- and untreated-SK-LU-1 cells. PCA was analyzed from the second derivative spectra of the 74, 88 and 55 spectra acquired from the control, sesamol- and cisplatin-treated SK-LU-1 cells, respectively, and presented as the PC1 and PC2 (Figure 5A).

Three clusters of spectra from the control, sesamol-, and cisplatin-treated SK-LU-1 cells were clearly separated into 2 dimensional score plots (PC1 *vs*. PC2) (Figure 5A). The cluster of untreated SK-LU-1 cells was clearly separated from the sesamol- and cisplatin-treated SK-LU-1 cells along PC1 (65%). The spectra of untreated and sesamol-treated SK-LU-1 cells were distinct from those of the cisplatin-treated SK-LU-1 cells along PC2 (21%) and the spectra of the sesamol- and cisplatin-treated SK-LU-1 cell clusters were clearly separated along PC2 (21%). Analyses of the PCA loading plots (Figure 5B and 5C) revealed the region of the FTIR spectra, which attributed significantly to the clustering (Figure 5A). The respective spectra of the sesamol- and cisplatin-treated SK-LU-1 cells were associated with positive scores in the score plot (PC1) and presented as negative loading of PC1.

The amide Ⅰ band of proteins at 1 660 cm^{-1} (assigned to the α-helix structure) was heavily loaded for PC1, which differentiated the spectra of the untreated cells from the spectra of the sesamol- and cisplatin-treated cells (Figure 5B). The control possessed a higher α-helix structure content than the sesamol- and cisplatin-treated cells. The β-sheet structure (1 631 cm^{-1}) was loaded for PC1 and indicated the β-sheet structure of the sesamol- and cisplatin-treated cells had a higher load than the untreated cells. In addition, the high negative value for PC1 loading at 1 649 cm^{-1} assigned to unordered random coils of amide Ⅰ was responsible for distinguishing the sesamol- and cisplatin-treated cells from the untreated cells.

The lipid region (3 000–2 800 cm^{-1}) was heavily loaded for PC2 at 2 925 cm^{-1} and 2 854 cm^{-1}, which distinguished the spectra of the sesamol and cisplatin-treated cells (Figure 5C), illustrating that the cisplatin-treated cells had higher lipid content than sesamol-treated cells. In addition, the negative values of PC1-loading at 2 919 cm^{-1} (assigned to the asymmetric stretching vibration of the CH_2- of the acyl chain in lipid) and 2 850 cm^{-1} (assigned to the symmetric stretching vibration of the CH_2- of the acyl chain in lipid) were responsible for differentiating the untreated cells from the treated cells. This result indicated that the lipid content of cisplatin-treated cells was higher than the untreated SK-LU-1 cells (Figure 5B and 5C).

In the nucleic acid region, the bands at 1 086 cm^{-1} and 1 084 cm^{-1} assigned to symmetric stretching of the phosphate groups ($\nu_s PO_2^-$) of phosphodiester bond in DNA and RNA were prominently loaded for PC1 (Figure 5B) and PC2 (Figure 5C), respectively. The positive value of PC1-loading at 1 086 cm^{-1} differentiated the untreated cells from the treated SK-LU-1 cells and the negative value of PC2-loading at 1 084 cm^{-1} differentiated the untreated cells and sesamol-treated cells from the cisplatin-treated cells (Figure 5A), illustrating that the untreated SK-LU-1 cells contributed to a greater nucleic acid content than the sesamol- and cisplatin-treated cells.

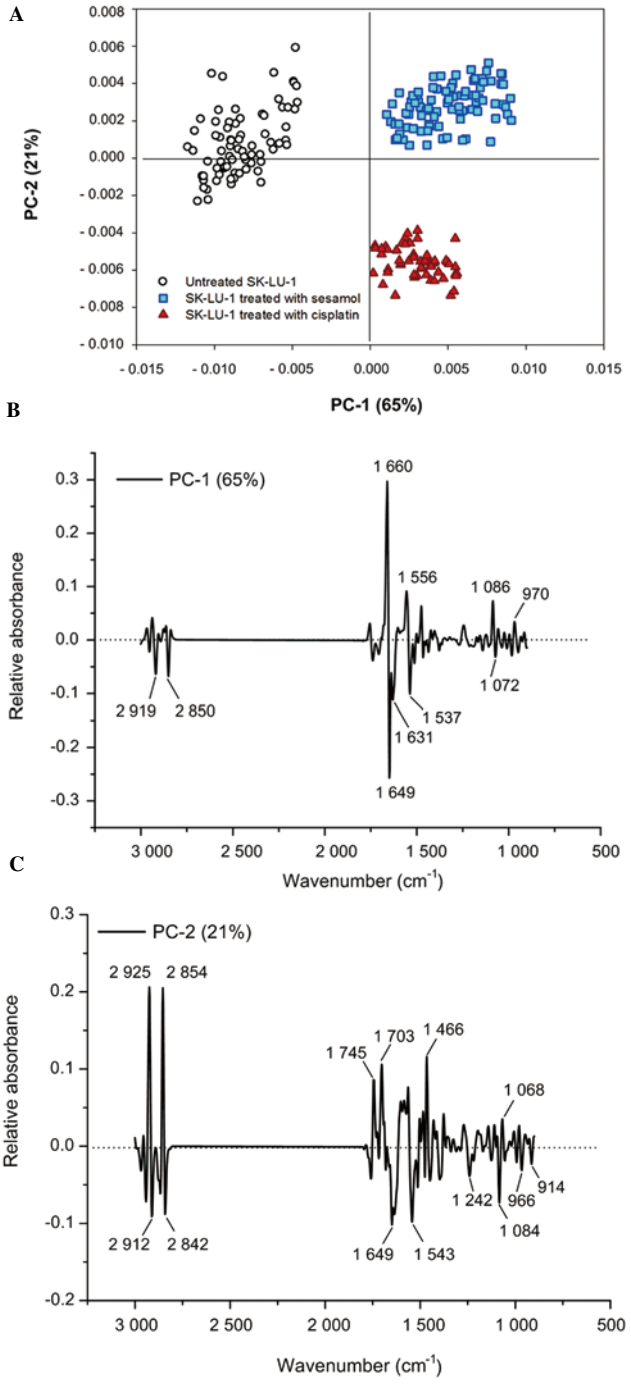

Figure 5. Principle component analysis of FTIR spectral with the range of 3 000–2 800 cm^{-1} and 1 800–900 cm^{-1}.
(A) PCA score plots, (B) and (C) PCA loading plots. PCA score plots show difference clustering between the untreated SK-LU-1 cells (o) and the SK-LU-1 cells treated with sesamol (■) and cisplatin (▲).

3.3. Alkylating activity

The current study determined the alkylating interaction of sesamol and cisplatin with DNA; based on colorimetric NBP assays. Figure 6 demonstrates that there was no color formation from pyridinium product detected for 5-FU, indicating there was no alkylation even using a concentration as high as 77 mM. Melphalan (30 mM) exerted

the highest alkylating activity. As expected, there was no alkylating activity for cisplatin (3 mM) observed which is likely due to the low concentration used. Although a 52-mM concentration of sesamol was used, it did not result in any positive alkylation under the conditions studied, ruling out alkylation by sesamol of DNA or of non-covalent binding. It is also evidenced that sesamol interacts on DNA through a different mechanism than cisplatin and melphalan.

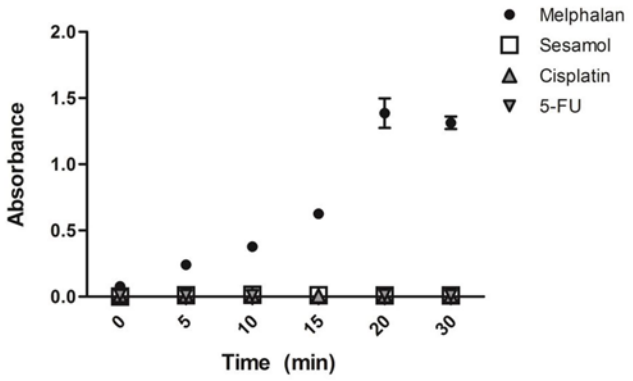

Figure 6. The NBP assay represented the alkylating interaction of melphalan (●), sesamol (□), cisplatin (▲) and 5-FU (▼).
Melphalan was used as a positive control. 5-FU was used as negative control. Data were represented as mean ± SD (n=3).

4. Discussion

Since DNA is one of the targets of chemotherapeutic drugs[18], many chemotherapeutic drugs induce cancer cell death by causing DNA damage leading to cell cycle arrest and apoptosis. DNA fragmentation is the one among apoptosis characteristics[19]. When cells undergo late stage apoptosis, the endonuclease enzyme is activated to cleave chromatin DNA into fragments of roughly 180-200 base pairs; resulting in DNA fragmentation or laddering. To investigate whether the cytotoxic effect of sesamol was due to apoptosis and associated with DNA, DNA fragmentation and cell cycle distribution were investigated. DNA laddering is a hallmark of cells undergoing apoptotic cell death. Apoptosis can be visualized due to DNA cleavage by the activation of a nuclear endonuclease at internucleosomal sites. The generating oligonucleosomal fragments can be observed as a ladder pattern of 180-200 bp by standard agarose gel electrophoresis[20,21].

Despite employing several techniques to monitor and assess the curative effect of chemotherapy *vs*. a natural compound on cancer; lung cancer is still the frequent cause of death in cancer patients. The present study demonstrated that the exposure of SK-LU-1 cells to sesamol induced a cascade of biochemical changes. We used FTIR microscopy to improve the assessment of cells after exposure to sesamol *vs*. cisplatin (an alkylating chemotherapeutic drug).

The FTIR microscopy technique uses infrared to interact with cells and detects the vibrational modes of the functional groups of cellular biomolecules[15]. Since the infrared spectrum of cells provides a precise image of all the chemical bonds that exist in the cell sample, FTIR microscopy has been used as an analytical tool for characterizing the action of therapeutic agents as indicated by different infrared fingerprints characteristics[22].

Cisplatin was previously reported to react with DNA via coordinate covalent bonds and hydrogen bonding[23]. The known anticancer mechanism of cisplatin is preferentially bound covalently to the N-7 position of guanine at the major groove of DNA producing cross-links[24]. Different cellular effects of cisplatin were reported in many cell lines. FTIR spectra of the MDA-MB-231 cells treated with cisplatin for 48 h clearly showed the changes at the DNA, lipid, and protein regions[25]. In protein region, amide Ⅰ band derives mainly from the C=O stretch vibrations of peptide linkages. The frequencies of the amide Ⅰ band components correlate to the secondary structure of proteins, while amide Ⅱ derives from in-plane NH-bending and CN-stretching vibration. Notwithstanding, amide Ⅱ reveals lesser protein conformational sensitivity than amide Ⅰ[26]. Cisplatin and sesamol exerted a significant effect on DNA conformation and on proteins. The metabolic changes such as high glycolysis and lipogenesis have been known in malignant cells in contrast to normal cells[27]. The cellular lipid components were more sensitive to cisplatin than sesamol. The increase in the lipid level has previously been reported in apoptotic cells to be associated with the exposure of the membrane phospholipid phosphatidylserine to the outer cell surface[15,28,29]. The cisplatin-protein interaction was represented by its effect on a protein (β-sheet)[30] and an increasing of relative amount of β-sheet, in accordance with the decreasing relative amount of α-helix, as per a previous study[28]. Cisplatin also decreased the nucleic acid content and caused a shift in a band of the DNA region, indicating the interaction between cisplatin and DNA bases (thymine, cytosine, guanine).

Melphalan is a bifunctional alkylating agent that is covalently bound to the nucleophilic sites in DNA such as N-7 of guanine[31]. Cisplatin was previously reported to intercalate with purine (guanine) bases of DNA through (i) strong electronic interaction between the Pt in cisplatin and N7-guanine[23], and (ii) the strong hydrogen bond between the hydrogen of the NH_3 of cisplatin and the oxo group at the C6 position of guanine[23,32]. The latter hydrogen bond crucially stabilized the cisplatin-guanine adduct.

Sesamol is a monophenolic compound with hydroquinone-like structure and it can form a strong hydrogen bond with the DNA base. Sesamol, however, contains no electrophilic site, so the covalent bond with the nucleophilic site on the DNA base—as with melphalan and cisplatin—did not occur. In a prior *in silico* molecular modeling study and *in vitro* study of sesamol with calf thymus DNA both reported that sesamol reacted with the DNA base at the minor groove with less DNA deformity because of the intercalation binding mode[4,33]. Notwithstanding, hydrogen bonding plays an important role for sesamol-targeted DNA. Sesamol and cisplatin interacted at different sites on the DNA base. Anticancer drugs have been reported to be small molecules[34] so a minor groove is the main target binding site of sesamol. According to the conducted experiments and previous reports of sesamol, sesamol affected the biochemical and physiological properties of SK-LU-1 cells. However, some cellular events were not detected by the experimental molecular biological techniques. In this study, sesamol did not exert alkylating activity by NBP assay although DNA fragmentation was evident as DNA ladder from gel electrophoresis corroborating with reduced DNA content in sub-G_1 phase. The result indicated that sesamol caused DNA damage via other mechanism. We, therefore, take advantage of FTIR microscopy technique to obtain additional biomedical information.

The results from the present study show that the relative integral area of the β-sheet was increased and the relative integral area of the α-helix was decreased. A similar change in the secondary protein structure when cells undergo apoptosis has been reported in

SK-LU-1 cells treated with cisplatin[28] and in U937 cells treated with melphalan[15]. Caspases and other pro-apoptotic protein members (such as TRAIL-R1, TRAIL-R2, and Bid) play major roles in apoptosis. The secondary structure of overexpressed TRAIL-R1 and TRAIL-R2 primarily comprises β-pleated sheets[35,36], while a decrease in expression of Bid, an α-structure, was observed[37]. The shift in position to a β-sheet may be related to conformational changes in these proteins during apoptosis[38]. Caspases are protease enzymes that regulate apoptotic cell death. The activation of caspases indicates the generation of death signals through both extrinsic and intrinsic apoptosis pathways. Sesamol was previously reported to significantly increase caspase 3/7 activities and overexpress pro-apoptotic proteins such as TRAIL-R1, TRAIL-R2 with a reduction of Bid in SK-LU-1 cells compared to the control[10]. The decrease in nucleic acid content is due to cancer cells undergoing apoptosis, resulting in inter-nucleosomal fragmentation of the genomic DNA-the biochemical marker of apoptosis[39].

As expected, different effects of sesamol and cisplatin on SK-LU-1 cells were reflected by the different FTIR spectra. Spectra are more or less affected by different treatments demonstrating different cell shapes, that is related to the cell status (different phases of the cell cycle, apoptotic or necrotic cells). We observed that sesamol induces alterations in the DNA and protein composition as well as secondary protein conformation in the SK-LU-1 cells, which in turn increased DNA damage according to the accumulation of the sub-G_1 phase and apoptosis induction mechanism. More elaborate work is underway to clarify the apoptosis induction mechanism behind these spectral changes. Notwithstanding, our major findings indicate that FTIR microscopy could be a useful tool for assessing mechanisms of anticancer action of sesamol compared with cisplatin. This FTIR microscopy is a well-established technique useful for the investigation of small cell sample. FTIR microscopy equipped with the mapping and imaging equipment allows one to collect large numbers of FTIR spectra and to assemble a pattern from sampling many different regions of the cell monolayer. Hence it is possible to assign band in the spectra of cells based on what changes occur upon treatment. FTIR microscopy allows us to distinguish apoptosis induction by sesamol from cisplatin in the SK-LU-1 cell line without labeling. It offers a promising alternative for monitoring cell alterations. Compared with established techniques, this method (a) provides distinctive biochemical information, (b) requires only minimal sample handling, (c) is relatively inexpensive, fast, and (d) can be automated with limited reagents. Specific DNA targeting underlying the apoptosis induction effect of sesamol was corroborated. In sum, applying both chemical and physiological detection methods on SK-LU-1 cell lines provides direction for elucidation of the mechanism of apoptosis induction action by sesamol.

FTIR microscopy, a novel technique in the field of cancer therapy, is able to distinguish apoptosis induction by sesamol from cisplatin in the mimic physiological condition in the SK-LU-1 cell line. The biochemical data demonstrated that sesamol and cisplatin induce apoptosis in SK-LU-1 cells by causing DNA damage resulting in DNA fragmentation. In addition, FTIR microscopic results revealed biomolecular alteration and DNA targeting effect of sesamol and cisplatin in SK-LU-1 cells.

Conflict of interest statement

The authors have no conflicts of interest to declare.

Acknowledgements

The authors are grateful for Mr. Bryan Roderick Hamman for editing the manuscript.

Funding

This work was supported by the Higher Education Research Promotion and National Research University Project of Thailand, Office of the Higher Education Commission, through the Food and Functional Food Research Cluster and Research and Development of Herbal Nutraceutics Subcluster of Khon Kaen University (FC 3.1.13 PhD and NRU 541057).

References

[1] Palchaudhuri R, Hergenrother PJ. DNA as a target for anticancer compounds: Methods to determine the mode of binding and the mechanism of action. *Curr Opin Biotechnol* 2007; **18**(6): 497-503.

[2] Gurova K. New hopes from old drugs: Revisiting DNA-binding small molecules as anticancer agents. *Future Oncol* 2009; **5**(10): 1685.

[3] Rauf S, Gooding JJ, Akhtar K, Ghauri MA, Rahman M, Anwar MA, et al. Electrochemical approach of anticancer drugs-DNA interaction. *J Pharm Biomed Anal* 2005; **37**(2): 205-217.

[4] Liu Z, Xiang Q, Du L, Song G, Wang Y, Liu X. The interaction of sesamol with DNA and cytotoxicity, apoptosis, and localization in HepG2 cells. *Food Chem* 2013; **141**(1): 289-296.

[5] Chen YH, Leu SF, Jen CY, Huang BM. Effects of sesamol on apoptosis and steroidogenesis in MA-10 mouse Leydig tumor cells. *J Agric Food Chem* 2011; **59**(18): 9885-9891.

[6] Miyahara Y, Hibasami H, Katsuzaki H, Imai K, Komiya T. Sesamol induces apoptosis in human lymphoid leukemia Molt 4B cells. *Food Sci Technol Res* 2000; **6**(3): 201-203.

[7] Kanimozhi P, Prasad NR. Antioxidant potential of sesamol and its role on radiation-induced DNA damage in whole-body irradiated Swiss albino mice. *Environ Toxicol Pharmacol* 2009; **28**(2): 192-197.

[8] Ramachandran S, Rajendra PN, Karthikeyan S. Sesamol inhibits UVB-induced ROS generation and subsequent oxidative damage in cultured human skin dermal fibroblasts. *Arch Dermatol Res* 2010; **302**(10): 733-744.

[9] Shanmugham M, Prasad N. Radiosensitizing effect of sesamol on human cervical carcinoma cells. *Int J Nutr Pharmacol Neurol Dis* 2012; **2**(3): 210.

[10]Siriwarin B, Weerapreeyakul N. Sesamol induced apoptotic effect in lung adenocarcinoma cells through both intrinsic and extrinsic pathways. *Chem-Biol Interact* 2016; **254**: 109-116.

[11]Dorraji PS, Jalali F. Investigation of the interaction of sertraline with calf thymus DNA by spectroscopic methods. *J Braz Chem Soc* 2013; **24**(6): 939-945.

[12]Sulé-Suso J, Skingsley D, Sockalingum GD, Kohler A, Kegelaer G, Manfait M, et al. FT-IR microspectroscopy as a tool to assess lung cancer cells response to chemotherapy. *Vib Spectrosc* 2005; **38**(1-2): 179-184.

[13]Junhom C, Weerapreeyakul N, Tanthanuch W, Thumanu K. FTIR microspectroscopy defines early drug resistant human hepatocellular

carcinoma (HepG2) cells. *Exp Cell Res* 2016; **340**(1): 71-80.

[14]Lee SY, Yoon KA, Jang SH, Ganbold EO, Uuriintuya D, Shin SM, et al. Infrared spectroscopy characterization of normal and lung cancer cells originated from epithelium. *J Vet Sci* 2009; **10**(4): 299-304.

[15]Machana S, Weerapreeyakul N, Barusrux S, Thumanu K, Tanthanuch W. FTIR microspectroscopy discriminates anticancer action on human leukemic cells by extracts of *Pinus kesiya*; *Cratoxylum formosum* ssp. pruniflorum and melphalan. *Talanta* 2012; **93**: 371-382.

[16]Srisayam M, Weerapreeyakul N, Barusrux S, Tanthanuch W, Thumanu K. Application of FTIR microspectroscopy for characterization of biomolecular changes in human melanoma cells treated by sesamol and kojic acid. *J Dermatol Sci* 2014; **73**(3): 241-250.

[17]Machana S, Weerapreeyakul N, Barusrux S, Nonpunya A, Sripanidkulchai B, Thitimetharoch T. Cytotoxic and apoptotic effects of six herbal plants against the human hepatocarcinoma (HepG2) cell line. *Chin Med* 2011; **6**(1): 39.

[18]Cheung-Ong K, Giaever G, Nislow C. DNA-damaging agents in cancer chemotherapy: Serendipity and chemical biology. *Chem Biol* 2013; **20**(5): 648-659.

[19]Kajstura M, Halicka HD, Pryjma J, Darzynkiewicz Z. Discontinuous fragmentation of nuclear DNA during apoptosis revealed by discrete "Sub-G_1" peaks on DNA content histograms. *Cytometry A* 2007; **71**(3): 125-131.

[20]Wyllie AH. Glucocorticoid-induced thymocyte apoptosis is associated with endogenous endonuclease activation. *Nature* 1980; **284**(5756): 555-556.

[21]Mizuta R, Araki S, Furukawa M, Furukawa Y, Ebara S, Shiokawa D, et al. DNase γ is the effector endonuclease for internucleosomal DNA fragmentation in necrosis. *PLoS One* 2013; **8**(12): e80223.

[22]Derenne A, Gasper R, Goormaghtigh E. The FTIR spectrum of prostate cancer cells allows the classification of anticancer drugs according to their mode of action. *Analyst* 2011; **136**(6): 1134-1141.

[23]Baik MH, Friesner RA, Lippard SJ. Theoretical study of cisplatin binding to purine bases: Why does cisplatin prefer guanine over adenine?. *J Am Chem Soc* 2003; **125**(46): 14082-14092.

[24]Dasari S, Tchounwou PB. Cisplatin in cancer therapy: Molecular mechanisms of action. *Eur J Pharmacol* 2014; **740**: 364-378.

[25]Batista de Carvalho ALM, Pilling M, Gardner P, Doherty J, Cinque G, Wehbe K, et al. Chemotherapeutic response to cisplatin-like drugs in human breast cancer cells probed by vibrational microspectroscopy. *Faraday Discuss* 2016; **187**: 273-298.

[26]Kong J, Yu S. Fourier transform infrared spectroscopic analysis of protein secondary structures. *Acta Bioch Bioph Sin* 2007; **39**(8): 549-559.

[27]Baenke F, Peck B, Miess H, Schulze A. Hooked on fat: The role of lipid synthesis in cancer metabolism and tumour development. *Dis Model Mech* 2013; **6**(6): 1353-1363.

[28]Plaimee P, Weerapreeyakul N, Thumanu K, Tanthanuch W, Barusrux S. Melatonin induces apoptosis through biomolecular changes, in SK-LU-1 human lung adenocarcinoma cells. *Cell Prolif* 2014; **47**(6): 564-577.

[29]Zelig U, Kapelushnik J, Moreh R, Mordechai S, Nathan I. Diagnosis of cell death by means of infrared spectroscopy. *Biophys J* 2009; **97**(7): 2107-2114.

[30]Farhadi E, Kobarfard F, Shirazi FH. FTIR biospectroscopy investigation on cisplatin cytotoxicity in three pairs of sensitive and resistant cell line. *Iran J Pharm Res* 2016; **15**(1): 213-220.

[31]Woods D, Turchi JJ. Chemotherapy induced DNA damage response: Convergence of drugs and pathways. *Cancer Biol Ther* 2013; **14**(5): 379-389.

[32]Chiavarino B, Crestoni ME, Fornarini S, Scuderi D, Salpin JY. Interaction of cisplatin with adenine and guanine: A combined IRMPD, MS/MS, and theoretical study. *J Am Chem Soc* 2013; **135**(4): 1445-1455.

[33]Kashanian S, Ghobadi AT, Roshanfekr H, Shariati Z. DNA interaction studies of sesamol (3,4-methylenedioxyphenol) food additive. *Mol Biol Rep* 2013; **40**(2): 1173-1179.

[34]Khan GS, Shah A, Zia ur R, Barker D. Chemistry of DNA minor groove binding agents. *J Photoch Photobio B* 2012; **115**: 105-118.

[35]Ramamurthy V, Yamniuk AP, Lawrence EJ, Yong W, Schneeweis LA, Cheng L, et al. The structure of the death receptor 4-TNF-related apoptosis-inducing ligand (DR4-TRAIL) complex. *Acta Cryst F* 2015; **71**(10): 1273-1281.

[36]Tamada T, Shinmi D, Ikeda M, Yonezawa Y, Kataoka S, Kuroki R, et al. TRAIL-R2 superoligomerization induced by human monoclonal agonistic antibody KMTR2. *Sci Rep* 2015; **5**: 17936.

[37]Chou JJ, Li H, Salvesen GS, Yuan J, Wagner G. Solution structure of BID, an intracellular amplifier of apoptotic signaling. *Cell* 1999; **96**(5): 615-624.

[38]Lavrik IN, Golks A, Krammer PH. Caspases: Pharmacological manipulation of cell death. *J Clin Invest* 2005; **115**(10): 2665-2672.

[39]Gasparri F, Muzio M. Monitoring of apoptosis of HL60 cells by Fourier-transform infrared spectroscopy. *Biochem J* 2003; **369**(2): 239-248.